Potts, D. M. & Zdravkovic, L. (2012). *Géotechnique* **62**, No. 12, 1053–1065 [http://dx.doi.org/10.1680/geot.11.P.057]

Accounting for partial material factors in numerical analysis

D. M. POTTS* and L. ZDRAVKOVIC*

The concept of a safety factor in the design of geotechnical structures has traditionally been developed within the framework of classical soil mechanics, where the analysis methods for its calculation involve simple limit equilibrium or limit analysis approaches. Therefore the inclusion of a safety factor within an advanced analysis method, such as finite elements or finite differences, is a more complex issue. In particular, the problem arises with design codes, such as Eurocode 7, in which partial factors on soil strength (or partial material factors) must be accounted for. Eurocode 7 implies that a numerical analysis should be performed accounting for a characteristic strength, which is reduced by partial factors. There are two ways in which such partial factors can be included in numerical analysis: one in which the strength is reduced at the beginning of the analysis, and the other in which this is done during the analysis. Eurocode 7 gives no guidance as to which one of these two approaches is more appropriate to apply. More importantly, there is no guidance on the appropriate numerical procedure that should be implemented in any software in order to perform the required strength reduction during the analysis in the latter approach. Therefore different software programs account for this in different ways, and mostly only for simple constitutive models. This paper presents, first, a consistent methodology for accounting for partial material factors in finite-element analysis, which can be applied to any constitutive model. It then demonstrates the implications of the two ways the partial material factors can be introduced in any analysis, using the example of a bearing capacity problem and employing constitutive models of increasing complexity. The paper shows that the two approaches for accounting for partial material factors may lead to different results, and that it is therefore necessary to develop a rational set of guidelines for their inclusion in advanced numerical analysis.

KEYWORDS: bearing capacity; constitutive relations; limit state design/analysis; numerical modelling

Le concept d'un facteur de sécurité dans l'étude de structures géotechniques a été développé traditionnellement dans le cadre de la mécanique classique des sols, dans laquelle les méthodes d'analyse pour son calcul comportent l'emploi de simples techniques d'équilibre limite ou d'analyse limite. En conséquence, l'inclusion d'un facteur de sécurité au sein d'une méthode d'analyse évoluée, par exemple une analyse aux éléments finis ou aux différences finies, est un problème plus complexe. Le problème se pose, en particulier, avec des codes d'étude, par exemple Eurocode 7, dans lesquels on doit tenir compte de facteurs partiaux sur la résistance des sols (ou des facteurs matériels partiels). Plus spécifiquement, Eurocode 7 implique que l'on doit effectuer une analyse numérique représentant une résistance caractéristique réduite par des facteurs partiels. Il est possible d'incorporer ces facteurs partiels dans l'analyse numérique de deux façons: en réduisant la résistance au début de l'analyse ou en la réduisant au cours de cette analyse. L'Eurocode 7 ne fournit aucune consigne sur la mieux appropriée de ces deux méthodes. En outre, et plus important encore, on ne dispose d'aucune consigne sur la procédure numérique appropriée qui doit être appliquée dans un logiciel quelconque, afin de procéder à la réduction de résistance requise au cours de l'analyse conformément à la dernière des méthodes susmentionnées. De ce fait, différents logiciels s'en acquittent de différentes façons, et, en général, simplement pour de simples modèles constitutifs. Cette communication présente une méthodologie homogène permettant de prendre en considération des facteurs de matériaux partiels dans des analyses aux éléments finis, qui peuvent être appliqués dans des modèles constitutifs quelconques. Elle démontre ensuite les implications des deux façons dont les facteurs matériels partiels peuvent être introduits dans une analyse sur l'exemple d'un problème de capacité portante, en employant des modèles constitutifs à complexité croissante. La communication indique que les deux méthodes permettant de prendre en considération des facteurs matériels partiels peuvent donner lieu à des résultats différents, et qu'il est par conséquent nécessaire de développer un ensemble de consignes rationnelles pouvant être incorporées dans des analyses numériques évoluées.

INTRODUCTION

Eurocode 7 (EC7) has been the primary geotechnical design code in Europe since 2010. It has effectively replaced the national design codes, albeit allowing for national annexes to the code to be introduced, which can still account for local practice. One of the main changes in the design practice introduced by EC7 is the introduction of partial factors on soil strength, resistance and applied loads. Three different design approaches (DA1, DA2 and DA3) are available in EC7, and each country has essentially adopted one of them. For example, the UK has selected to use approach DA1. These approaches differ, in that different magnitudes and combinations of partial factors are employed. For example, the partial factors recommended for soil strength are given in Table 1. Design approach 2 (DA2) is the only one that does not involve partial factors on soil strength, whereas both DA1 and DA3 account for partial factors on both drained conditions (represented by the cohesion, c', and the angle of shearing resistance, ϕ', strength parameters), and the undrained conditions (represented by the undrained strength, S_u). Where and how the partial factors are applied in the design of geotechnical structures has been discussed, among others, by Simpson (2000), Bauduin *et al.* (2003), Simpson (2007) and Cheung *et al.* (2010).

Manuscript received 24 May 2011; revised manuscript accepted 21 March 2012. Published online ahead of print 3 September 2012. Discussion on this paper closes on 1 May 2013, for further details see p. ii.

* Imperial College London, UK.

Table 1. Partial factors for soil strength as recommended by EC7

EC7 design approach	$\tan\phi'$	c'	Undrained strength
DA1/1	1·0	1·0	1·0
DA1/2	1·25	1·25	1·4
DA2	1·0	1·0	1·0
DA3	1·25	1·25	1·4

An additional challenge of EC7 is that it is not as prescriptive of the type of geotechnical analysis to be used in design as was the case with previous codes, and encourages the use of numerical analysis (e.g. finite elements or finite differences). However, it does not provide guidance as to how the partial factors should be applied in numerical analysis. For example, the introduction of partial factors on soil strength, or partial material factors, implies that the soil's characteristic strength should be reduced by the relevant partial factor, and this can be achieved in one of two ways: at a suitable stage during an analysis (termed here the SR1 approach), or at the beginning of an analysis (termed the SR2 approach). There is no guidance on which of these two approaches is more appropriate to apply, or on the appropriate numerical procedure for strength reduction in the former approach (SR1). Some of these issues have been investigated by Bauduin *et al.* (2000), Schweiger (2005), Schweiger *et al.* (2010) and Potts & Zdravkovic (2011), but with a limited scope. With respect to the SR1 approach, attempts have been made in the past to calculate safety factors in numerical analysis (e.g. Brinkgreve & Bakker, 1991). However, these procedures consider only simple constitutive models of the Mohr–Coulomb type, and rely on the stress-point algorithm to adjust the stress state from the initial yield surface to the new yield surface that corresponds to smaller strength. Such procedures can be problematic, particularly for more complex constitutive models.

The subject of the current paper is the application of partial material factors in numerical analysis. It first discusses the two possible approaches for strength reduction (SR1 and SR2), and their advantages and disadvantages. It then presents a consistent numerical procedure for strength-reduction approach SR1 within the finite-element formulation, which can be implemented in any software and for any soil's constitutive model. Finally, the implications of the two approaches are demonstrated and discussed on an example of the bearing capacity analysis of a strip footing on a homogeneous soil, employing constitutive models of increasing complexity: Tresca, modified Cam-Clay (MCC) and Lade's single-hardening models. These analyses have been performed with the finite-element software ICFEP (Potts & Zdravkovic, 1999), which employs a modified Newton–Raphson non-linear solver with an error-controlled substepping stress-point algorithm.

AVAILABLE APPROACHES FOR PARTIAL MATERIAL FACTORS IN NUMERICAL ANALYSIS

The application of partial material factors implies that the material design strength used in an analysis is based on the characteristic strength, but reduced by partial factors. The characteristic strength is the best estimate of the soil's strength from the available site investigation data. The derivation of the characteristic strength is a separate issue within the EC7 design procedure, and is not the subject of the current paper.

For geotechnical problems that are dominated by undrained behaviour, and where a total stress constitutive model using the undrained strength S_u is employed, the application of partial factors implies that the design (factored) strength used in an analysis, $S_{u,d}$, is estimated as

$$S_{u,d} = \frac{S_{u,ch}}{\gamma_m} \tag{1}$$

whereas for problems based on drained strength – the angle of shearing resistance ϕ' and cohesion c' – the design (factored) strength used in an analysis, ϕ'_d and c'_d, is estimated as

$$\phi'_d = \arctan\left(\frac{\tan\phi'_{ch}}{\gamma_m}\right)$$
$$c'_d = \frac{c'_{ch}}{\gamma_m} \tag{2}$$

In the above equations γ_m is a partial material factor, and $S_{u,ch}$, ϕ'_{ch} and c'_{ch} are the characteristic (unfactored) values of soil strength, estimated from the site investigation data. The strength reduction given by these equations can be achieved in two ways in numerical analysis, which both have advantages and disadvantages in their application.

The first approach, SR1, is to start the analysis with the characteristic strength ($S_{u,ch}$ or ϕ'_{ch} and c'_{ch} as applicable) directly, without modification, and then at relevant stages of the analysis to gradually increase the partial material factor (i.e. to reduce the strength), until failure in the soil is fully mobilised. The advantage of this strength-reduction approach is that a single analysis could be used for assessing both the serviceability and ultimate limit states for the problem being analysed. It is also possible to obtain, from this single analysis, the magnitude of the factor of safety at the ultimate limit state (i.e. collapse). However, the disadvantage of this approach is that it requires modification of the numerical software. As there is no agreed unique way of how this strength reduction should be numerically implemented, different software accounts for it in different ways, which are not always clearly explained. Also, most software can perform such reductions only if simple constitutive models are used in the analysis. However, as shown subsequently, this approach has the potential for being used with most, if not all, constitutive models.

The second approach, SR2, is to start the analysis with the factored strength ($S_{u,d}$ or ϕ'_d and c'_d), as given by equation (1) or equation (2), and continue until the analysis is completed. The advantage of this approach is that no modification to the analysis software is needed, which makes it an easier option to use. The disadvantage is that such a reduced strength may require initial stresses that are not consistent with those in situ, resulting, for example, in wrong structural forces being calculated in retaining walls or tunnel linings that are present in the analysis. In addition, in an analysis with the SR2 approach, all stages of the analysis may be completed without reaching failure, which ensures the stability of the problem, but does not produce information on the real magnitude of the safety factor. Another disadvantage of this approach is that it may not be easy to use in combination with advanced constitutive models in which strength is stress and/or strain dependent.

An additional issue with the two strength-reduction approaches is whether they produce the same result for a given problem (i.e. the same limit state). This will be investigated in the following sections of the paper by considering the results of bearing capacity analyses using three different constitutive models.

NUMERICAL IMPLEMENTATION OF STRENGTH-REDUCTION APPROACH SR1

The theory presented in this section has been derived for constitutive models with a single yield surface (e.g. Tresca, Mohr–Coulomb, MCC). A similar procedure applies for models with two or more yield surfaces.

In the proposed procedure it is recognised that, to account for a partial material factor in the finite-element formulation, it is necessary to (a) derive a new relationship between the change in stresses and change in total strains, and (b) modify the governing finite-element equations. Both of these changes are derived below.

Relationship between changes in stresses and strains

In a conventional elasto-plastic constitutive model, which does not account for a partial material factor, the yield surface is a function of stresses and state parameters, usually written in the form

$$F(\{\sigma\}, \{k\}) = 0 \tag{3}$$

where $\{\sigma\}$ is the stress vector and $\{k\}$ is the vector of state parameters. For such a model the change in stresses, $\{\Delta\sigma\}$, is related to the change in total strains, $\{\Delta\varepsilon\}$, via the elasto-plastic constitutive matrix $[D^{ep}]$ (e.g. Potts & Zdravkovic, 1999)

$$\{\Delta\sigma\} = [D^{ep}] \cdot \{\Delta\varepsilon\} \tag{4}$$

If the partial material factor, γ_m, is to be included in a constitutive model, the novel idea presented in the current paper is to consider γ_m as an additional state parameter, in a scalar form, such that the yield function is expressed as

$$F(\{\sigma\}, \{k\}, \gamma_m) = 0 \tag{5}$$

The default value of γ_m is 1·0, and it increases incrementally at a desired stage of the analysis. It is now necessary to derive the relationship between the changes in stresses and total strains, similar to equation (4), which will account for the changing partial material factor.

In line with standard elasto-plasticity, the change in total strains, $\{\Delta\varepsilon\}$, can be split into elastic, $\{\Delta\varepsilon^e\}$, and plastic, $\{\Delta\varepsilon^p\}$, components to give

$$\{\Delta\varepsilon\} = \{\Delta\varepsilon^e\} + \{\Delta\varepsilon^p\} \tag{6}$$

The change in stresses, $\{\Delta\sigma\}$, is then related to the change in elastic strains, $\{\Delta\varepsilon^e\}$, by the elastic constitutive matrix, $[D]$, in the form

$$\{\Delta\sigma\} = [D] \cdot \{\Delta\varepsilon^e\} \tag{7}$$

Combining equations (6) and (7) gives

$$\{\Delta\sigma\} = [D] \cdot (\{\Delta\varepsilon\} - \{\Delta\varepsilon^p\}) \tag{8}$$

The change in plastic strains, $\{\Delta\varepsilon^p\}$, is related to the plastic potential function, $P(\{\sigma\}, \{m\}) = 0$, where $\{m\}$ are state parameters, via a flow rule that can be written as

$$\{\Delta\varepsilon^p\} = \Lambda \cdot \left\{\frac{\partial P(\{\sigma\}, \{m\})}{\partial\sigma}\right\} \tag{9}$$

where Λ is a scalar multiplier. Substituting equation (9) into equation (8) gives

$$\{\Delta\sigma\} = [D] \cdot \{\Delta\varepsilon\} - \Lambda \cdot [D] \cdot \left\{\frac{\partial P(\{\sigma\}, \{m\})}{\partial\sigma}\right\} \tag{10}$$

When the material is plastic, the stress state must satisfy the yield function $F(\{\sigma\}, \{k\}, \gamma_m) = 0$. Consequently, the total differential of the yield function, $dF(\{\sigma\}, \{k\}, \gamma_m\})$, must also equal 0, which, on using the chain rule of differentiation, gives

$$dF(\{\sigma\}, \{k\}, \gamma_m) = \left\{\frac{\partial F(\{\sigma\}, \{k\}, \gamma_m)}{\partial\sigma}\right\}^T \cdot \{\Delta\sigma\} + \left\{\frac{\partial F(\{\sigma\}, \{k\}, \gamma_m)}{\partial k}\right\}^T \cdot \{\Delta k\} + \frac{\partial F(\{\sigma\}, \{k\}, \gamma_m)}{\partial\gamma_m} \cdot \Delta\gamma_m = 0 \tag{11}$$

Equation (11) is known as the consistency equation or condition, which can be rearranged to give

$$\{\Delta\sigma\} = -\frac{\left\{\frac{\partial F(\{\sigma\}, \{k\}, \gamma_m)}{\partial k}\right\}^T \cdot \{\Delta k\} + \frac{\partial F(\{\sigma\}, \{k\}, \gamma_m)}{\partial\gamma_m} \cdot \Delta\gamma_m}{\left\{\frac{\partial F(\{\sigma\}, \{k\}, \gamma_m)}{\partial\sigma}\right\}^T} \tag{12}$$

Combining equations (10) and (12) makes it possible to calculate the scalar multiplier Λ

$$\Lambda = \frac{\left\{\frac{\partial F(\{\sigma\}, \{k\}, \gamma_m)}{\partial\sigma}\right\}^T \cdot [D] \cdot \{\Delta\varepsilon\} + \frac{\partial F(\{\sigma\}, \{k\}, \gamma_m)}{\partial\gamma_m} \cdot \Delta\gamma_m}{\left\{\frac{\partial F(\{\sigma\}, \{k\}, \gamma_m)}{\partial\sigma}\right\}^T \cdot [D] \cdot \left\{\frac{\partial P(\{\sigma\}, \{m\})}{\partial\sigma}\right\} + A} \tag{13}$$

where

$$A = -\frac{1}{\Lambda} \cdot \left\{\frac{\partial F(\{\sigma\}, \{k\}, \gamma_m)}{\partial k}\right\}^T \cdot \{\Delta k\} \tag{14}$$

Substituting equation (13) into equation (10) gives the final expression for the change in stresses

$$\{\Delta\sigma\} = \left[[D] - \frac{[D] \cdot \left\{\frac{\partial P(\{\sigma\}, \{m\})}{\partial\sigma}\right\} \cdot \left\{\frac{\partial F(\{\sigma\}, \{k\}, \gamma_m)}{\partial\sigma}\right\}^T \cdot [D]}{\left\{\frac{\partial F(\{\sigma\}, \{k\}, \gamma_m)}{\partial\sigma}\right\}^T \cdot [D] \cdot \left\{\frac{\partial P(\{\sigma\}, \{m\})}{\partial\sigma}\right\} + A}\right] \cdot \{\Delta\varepsilon\} - \frac{[D] \cdot \left\{\frac{\partial P(\{\sigma\}, \{m\})}{\partial\sigma}\right\} \cdot \frac{\partial F(\{\sigma\}, \{k\}, \gamma_m)}{\partial\gamma_m} \cdot \Delta\gamma_m}{\left\{\frac{\partial F(\{\sigma\}, \{k\}, \gamma_m)}{\partial\sigma}\right\}^T \cdot [D] \cdot \left\{\frac{\partial P(\{\sigma\}, \{m\})}{\partial\sigma}\right\} + A} \tag{15}$$

which can be rewritten in the following form, similar to equation (4)

$$\{\Delta\sigma\} = [D^{ep}] \cdot \{\Delta\varepsilon\} - \{\Delta\sigma_c\} \tag{16}$$

with

$$[D^{\mathrm{ep}}] = [D] - \frac{[D]\cdot\left\{\dfrac{\partial P(\{\sigma\},\{m\})}{\partial\sigma}\right\}\cdot\left\{\dfrac{\partial F(\{\sigma\},\{k\},\gamma_{\mathrm{m}})}{\partial\sigma}\right\}^{\mathrm{T}}\cdot[D]}{\left\{\dfrac{\partial F(\{\sigma\},\{k\},\gamma_{\mathrm{m}})}{\partial\sigma}\right\}^{\mathrm{T}}\cdot[D]\cdot\left\{\dfrac{\partial P(\{\sigma\},\{m\})}{\partial\sigma}\right\}+A} \tag{17}$$

and

$$\{\Delta\sigma_{\mathrm{c}}\} = \frac{[D]\cdot\left\{\dfrac{\partial P(\{\sigma\},\{m\})}{\partial\sigma}\right\}\cdot\dfrac{\partial F(\{\sigma\},\{k\},\gamma_{\mathrm{m}})}{\partial\gamma_{\mathrm{m}}}\cdot\Delta\gamma_{\mathrm{m}}}{\left\{\dfrac{\partial F(\{\sigma\},\{k\},\gamma_{\mathrm{m}})}{\partial\sigma}\right\}^{\mathrm{T}}\cdot[D]\cdot\left\{\dfrac{\partial P(\{\sigma\},\{m\})}{\partial\sigma}\right\}+A} \tag{18}$$

The definition of the $[D^{\mathrm{ep}}]$ matrix derived in equation (17) is identical to that of an elasto-plastic model that does not include a partial material factor (e.g. Potts & Zdravkovic, 1999). The vector $\{\Delta\sigma_{\mathrm{c}}\}$ represents the reduction in stresses due to the imposed incremental increase in the partial material factor and a consequent reduction in material strength. If the partial factor is constant, then $\Delta\gamma_{\mathrm{m}} = 0$ and $\{\Delta\sigma_{\mathrm{c}}\} = 0$. It also remains that if purely elastic behaviour is being experienced then $[D^{\mathrm{ep}}]$ reduces to the elastic matrix $[D]$, and again $\{\Delta\sigma_{\mathrm{c}}\} = 0$.

Effect on governing finite-element equations

Adopting the conventional procedure described in Potts & Zdravkovic (1999), for example, the governing finite-element equations are derived using the principle of minimum potential energy. This principle states that the static equilibrium position of a loaded body is the one that minimises the total potential energy, defined as

$$\text{Total potential energy } (E) = \text{Strain energy } (W) - \text{Work done by applied loads } (L) \tag{19}$$

Consequently, the principle of minimum potential energy states that, for equilibrium

$$\delta\Delta E = \delta\Delta W - \delta\Delta L = 0 \tag{20}$$

The strain energy, ΔW, or the work done by internal forces (stresses), can be written as

$$\Delta W = \frac{1}{2}\int_{Vol}\{\Delta\varepsilon\}^{\mathrm{T}}\cdot\{\Delta\sigma\}\mathrm{d}Vol \tag{21}$$

where the integration is over the volume of the body. Substituting equation (16) into equation (21) gives

$$\Delta W = \frac{1}{2}\int_{Vol}\{\Delta\varepsilon\}^{\mathrm{T}}\cdot\left([D^{\mathrm{ep}}]\cdot\{\Delta\varepsilon\} - \{\Delta\sigma_{\mathrm{c}}\}\right)\mathrm{d}Vol \tag{22}$$

The work done by the applied loads, ΔL, or the external work, can be divided into contributions from body forces and surface tractions, and can therefore be expressed as

$$\Delta L = \int_{Vol}\{\Delta d\}^{\mathrm{T}}\cdot\{\Delta F\}\ \mathrm{d}Vol + \int_{Srf}\{\Delta d\}^{\mathrm{T}}\cdot\{\Delta T\}\ \mathrm{d}Srf \tag{23}$$

where: $\{\Delta d\}$ is the vector of displacements; $\{\Delta F\}$ is the vector of body forces; $\{\Delta T\}$ is the vector of surface tractions (line loads, surcharge pressure, etc.); and *Srf* is that part of the boundary of the domain over which the surface tractions are applied.

The incremental total potential energy of the body is then given as

$$\Delta E = \frac{1}{2}\int_{Vol}\{\Delta\varepsilon\}^{\mathrm{T}}\cdot\left([D^{\mathrm{ep}}]\cdot\{\Delta\varepsilon\} - \{\Delta\sigma_{\mathrm{c}}\}\right)\mathrm{d}Vol - \int_{Vol}\{\Delta d\}^{\mathrm{T}}\cdot\{\Delta F\}\mathrm{d}Vol - \int_{Srf}\{\Delta d\}^{\mathrm{T}}\cdot\{\Delta T\}\mathrm{d}Srf \tag{24}$$

Considering that a finite-element mesh is an assembly of a number of individual finite elements, the potential energy of the whole system is the sum of the potential energies of the separate elements

$$\Delta E = \sum_{i=1}^{N}\Delta E_i \tag{25}$$

where N is the number of elements. In addition, the variation of displacements $\{\Delta d\}$ across a single element can be expressed in terms of nodal values of displacements, which leads to

$$\{\Delta d\} = [N]\cdot\{\Delta d\}_{\mathrm{n}} \tag{25a}$$

and

$$\{\Delta\varepsilon\} = [B]\cdot\{\Delta d\}_{\mathrm{n}} \tag{25b}$$

where $[N]$ is the matrix of shape functions, $[B]$ is the matrix of derivatives of the shape functions, and $\{\Delta d\}_{\mathrm{n}}$ is the vector of nodal displacements for a single element. By substituting this into equation (24), the potential energy is obtained as

$$\Delta E = \sum_{i=1}^{N}\left[\frac{1}{2}\int_{Vol}\Big(\{\Delta d\}_{\mathrm{n}}^{\mathrm{T}}\cdot[B]^{\mathrm{T}}\cdot[D^{\mathrm{ep}}]\cdot[B]\cdot\{\Delta d\}_{\mathrm{n}} - \{\Delta d\}_{\mathrm{n}}^{\mathrm{T}}\cdot[B]^{\mathrm{T}}\cdot\{\Delta\sigma_{\mathrm{c}}\} - 2\cdot\{\Delta d\}_{\mathrm{n}}^{\mathrm{T}}\cdot[N]^{\mathrm{T}}\cdot\{\Delta F\}\Big)\mathrm{d}Vol - \int_{Srf}\{\Delta d\}_{\mathrm{n}}^{\mathrm{T}}\cdot[N]^{\mathrm{T}}\{\Delta T\}\mathrm{d}Srf\right] \tag{26}$$

where the volume integrals are now performed over the volume of an element (d*Vol*), and the surface integral is performed over that portion of the element boundary (d*Srf*) over which surface tractions are specified. The principal unknowns are the incremental nodal displacements over that element. Minimising the potential energy with respect to these incremental nodal displacements gives the governing finite-element equation

$$\sum_{i=1}^{N}[K_{\mathrm{E}}]_i\cdot\left(\{\Delta d\}_{\mathrm{n}}\right)_i = \sum_{i=1}^{N}\{\Delta R_i\} \tag{27}$$

where

$$[K_{\mathrm{E}}] = \int_{Vol}[B]^{\mathrm{T}}\cdot[D^{\mathrm{ep}}]\cdot[B]\mathrm{d}Vol$$

is the element stiffness matrix, and

$$\{\Delta R_E\} = \int_{Vol} [N]^T \cdot \{\Delta F\} dVol + \int_{Srf} [N]^T \cdot \{\Delta T\} dSrf + \frac{1}{2}\int_{Vol} [B]^T \cdot \{\Delta \sigma_c\} dVol$$

is the right-hand-side load vector.

Equation (27) is similar to the conventional equation derived in Potts & Zdravkovic (1999), but with the addition of the third term (related to $\{\Delta\sigma_c\}$) in the right-hand-side load vector, which represents the effect of changing the partial material factor. Consequently, if only the partial material factor changes (i.e. $\{\Delta F\} = \{\Delta T\} = 0$), there is still a non-zero right-hand-side vector that initiates changes in displacements, and therefore in stresses and strains too.

In summary, the above proposed procedure for inclusion of a partial material factor in finite-element analysis requires a straightforward modification of the finite-element formulation. First, the relationship between the changes in stresses and strains is the same as in a standard elasto-plastic constitutive model with a single yield surface, but reduced by the vector $\{\Delta\sigma_c\}$. Second, the governing finite-element equation is the same as in a standard finite-element formulation, with the only difference being that the right-hand-side vector now has the addition of a term containing the vector $\{\Delta\sigma_c\}$. The expression for $\{\Delta\sigma_c\}$ is derived in equation (18), where it can be seen that, apart from the usual derivatives of the yield and plastic potential functions of the model with respect to stresses, a derivative of the yield function with respect to the partial material factor is also needed. For the constitutive models applied in the bearing capacity study presented here (i.e. Tresca, MCC and Lade's single hardening), the $(\partial F(\{\sigma\},\{k\},\gamma_m)/\partial\gamma_m)$ derivatives are presented in the Appendix.

In the analyses performed for this paper, the $\{\Delta\sigma_c\}$ in the right-hand-side load vector of equation (27) was calculated using the stress state corresponding to the beginning of an increment. During the subsequent modified Newton–Raphson iterative process, the $\{\Delta\sigma_c\}$ used to obtain the changes in stresses from the changes in strains in the stress-point algorithm accounts for the changes in stress and partial material factor over the whole increment (i.e. an error-controlled substepping scheme is used; see Potts & Zdravkovic, 1999).

FINITE-ELEMENT MODEL OF A BEARING CAPACITY PROBLEM

The above procedure for accounting for a partial material factor in a finite-element analysis was implemented in the finite-element software ICFEP (Potts & Zdravkovic, 1999), which is applied here in the analyses of a bearing capacity problem of a rough and rigid strip footing. The objective of the study is to investigate the application of strength-reduction approaches SR1 and SR2 with constitutive models of increasing complexity.

The Tresca model is one of the simplest constitutive models, formulated in terms of total stresses, where the soil's strength is characterised by the undrained strength S_u. MCC is a critical-state-based, strain-hardening/softening, effective stress model, with the soil's strength expressed in terms of the angle of shearing resistance ϕ'. Finally, Lade's single-hardening model is also a strain-hardening/softening effective stress model, with both the ϕ' and c' (cohesion) strength parameters. More importantly, ϕ' is not a constant value (as in the MCC model), but varies with stress and strain level, and is not a direct input parameter to the model. Details of these three constitutive models are not presented here, as this information can be found elsewhere in the literature. In particular, Potts & Zdravkovic (1999) describe all three models in the forms in which they have been implemented in ICFEP. Other references include Roscoe & Burland (1968) for the MCC model, and Kim & Lade (1988), Lade & Kim (1988) and Kovacevic (1994) for Lade's model.

The geometry of the problem being analysed is shown by the finite-element mesh in Fig. 1. The strip footing is 2 m wide, and because of symmetry in both its geometry and loading conditions (i.e. vertical load), only half of the problem is discretised in Fig. 1. The footing itself is not discretised in the mesh. Its rough interface is simulated by prescribing zero horizontal displacements at the nodes at the soil/footing interface, whereas the rigid conditions are simulated by the uniform incremental vertical displacements applied at the same nodes. The vertical load on the footing is then calculated from the reactions to the prescribed vertical displacements. The remaining boundary conditions are those of prescribed zero horizontal displacements and vertical forces on the two vertical boundaries of the problem, and zero vertical and horizontal displacements on the bottom boundary. The top boundary away from the footing edge is stress free. The soil domain is considered homogeneous in all analyses. Both drained and undrained bearing capacities of this footing are considered in the following analyses.

Model parameters and ground conditions

The first set of analyses is performed with the Tresca constitutive model. The undrained strength is assumed constant with depth, with $S_{u,ch} = 100$ kPa. A Poisson's ratio of 0·499 and an undrained Young's modulus of 10^5 kPa are assumed in the analyses. The initial stresses in the ground assume a bulk unit weight $\gamma = 20$ kN/m^3 and a $K_0 = 1$ on total stresses in all analyses. Only undrained bearing capacity analyses are performed with this model.

Analyses with the MCC constitutive model assume the soil to be normally consolidated (i.e. OCR = 1), with the groundwater table (GWT) 2 m below the ground surface. A hydrostatic pore water pressure profile is adopted, which gives suction above the GWT, and the bulk unit weight of the soil $\gamma = 20$ kN/m^3. The adopted K_0 values vary between different analyses, which is explained later. The form of the MCC model used in these analyses adopts the Mohr–

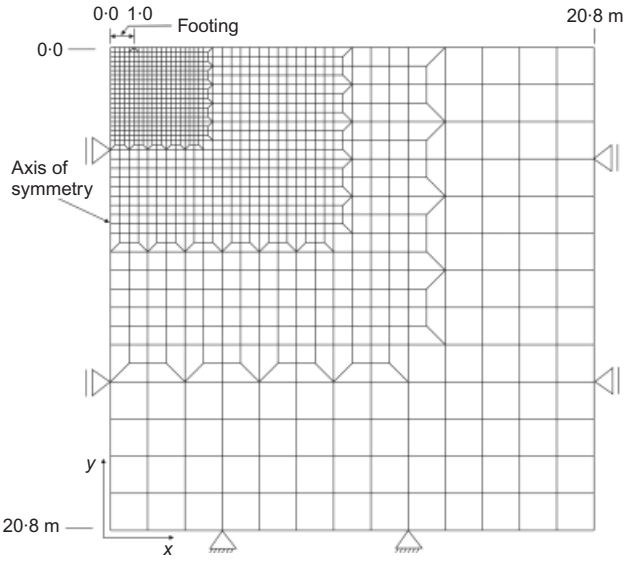

Fig. 1. Finite-element mesh for bearing capacity problem

Table 2. Input parameters for MCC model

Parameter	Value
Inclination of virgin compression line in v–$\ln p'$ space, λ	0·16
Inclination of swelling lines in v–$\ln p'$ space, κ	0·02
Specific volume at unit mean effective stress, v_1	3·2
Poisson's ratio, μ	0·3
Angle of shearing resistance, ϕ'_{ch}: degrees	30

Coulomb hexagon for the shape of the yield surface, and a circle for the shape of the plastic potential surface in the deviatoric plane. The relevant strength parameter $\phi'_{ch} = 30°$ is assumed. The remaining parameters for this model are summarised in Table 2. These parameters have been adopted from the calibration of a normally consolidated soft clay soil described in Zdravkovic *et al.* (2003). Both drained and undrained bearing capacity analyses are performed with this model.

Analyses with Lade's single-hardening model also assume the soil to be normally consolidated (i.e. OCR = 1). The model parameters are summarised in Table 3, and are taken from the calibration of a fine silica sand by Lade & Kim (1988) and Kovacevic (1994). Dry sand is considered in the analyses, with the bulk unit weight of the sand $\gamma = 20$ kN/m^3, a surcharge load of 10 kPa on the ground surface, and $K_0 = 0{\cdot}4$ throughout. Only drained bearing capacity analyses are considered with this model.

UNDRAINED BEARING CAPACITY

The undrained bearing capacity of the above strip footing is considered first, applying both the Tresca and MCC constitutive models. The undrained conditions are implicit in the Tresca model, owing to its formulation in terms of total stresses. An effective stress model, like the MCC, is applied in the analysis of an undrained problem when it is necessary to monitor the changes in both the effective stresses and pore water pressures in the ground, which is not possible with a simple, total-stress-based Tresca model. It is also applied in an analysis in which both the short- and long-term behaviour are being investigated. The approach adopted here for the simulation of undrained conditions with the effective stress model is that of prescribing a large value for the compressibility of the pore fluid (see Potts & Zdravkovic, 1999, for further explanation).

Table 3. Input parameters for Lade's single-hardening model

Parameter	Value
Young's modulus coefficient, M	1170
Young's modulus exponent, λ	0·53
Poisson's ratio, μ	0·2
Failure constant, $\eta_{1,ch}$	24·7
Failure exponent, m	0·1
Plastic potential coefficient, ψ_2	−3·69
Plastic potential exponent, g	2·26
Work-hardening parameter, C	0·000324
Work-hardening exponent, p	1·25
Yield exponent, h	0·355
Yield parameter, α	0·515

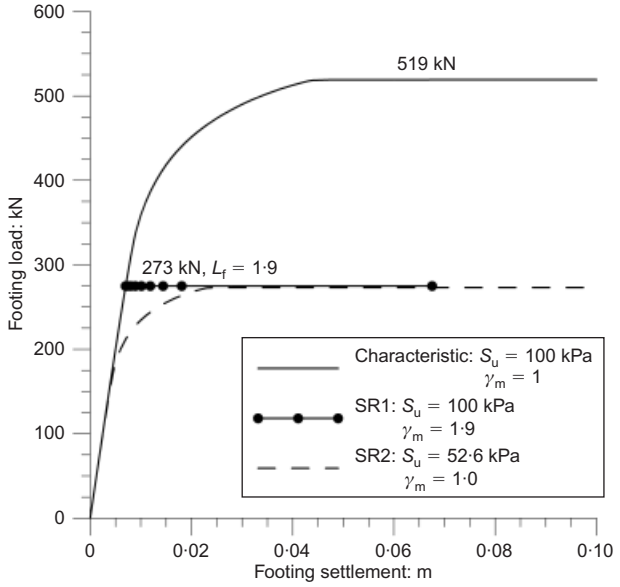

Fig. 2. Load–settlement curves for undrained footing capacity using Tresca model

Analysis results with Tresca model

The first analysis of the above strip footing using the Tresca constitutive model adopted the characteristic strength in the soil $S_{u,ch} = 100$ kPa. The resulting load–settlement curve for the footing is shown in Fig. 2 as a solid line. The predicted ultimate load on the footing is $Q_f = 519$ kN, which results in the bearing capacity factor $N_c = 5{\cdot}19$ ($= Q_f/(A.S_u)$, where A is the base area of the footing, 1 m^2 in this case). This result is within 1% of the theoretical value of the bearing capacity factor $N_c = 5{\cdot}14$, which confirms sufficient accuracy of the analysis procedure for this problem.

In the second analysis strength-reduction approach SR1 is applied, in that the characteristic strength in the soil $S_{u,ch} = 100$ kPa is adopted at the beginning of the analysis. The footing is initially loaded to a working load of 273 kN, which represents a load factor, L_f, of 1·9 with respect to the ultimate load (i.e. $L_f = 519/273$). This load was then maintained in the analysis while the partial material factor was incrementally increased (i.e. the undrained strength was reduced), following the numerical procedure introduced in the previous sections of this paper, until failure occurred. Failure was identified when equilibrium could not be maintained, and large displacements were occurring. The load–displacement curve (solid line with symbols) in Fig. 2 shows that the footing deforms further while the load is maintained, owing to the reduction in the soil's strength. The resulting partial material factor, γ_m, was 1·9, which is identical to the load factor for the applied working load, as would be expected.

The final analysis then applied strength-reduction approach SR2, such that the undrained strength at the beginning of this analysis was reduced by the partial material factor 1·9 obtained in the second analysis: that is, $S_{u,d} = 100/1{\cdot}9 = 52{\cdot}6$ kPa. The footing was then loaded to failure with this undrained strength in the soil, resulting in the ultimate load of 273 kN, as shown by the dashed line in Fig. 2.

These analyses showed that with the Tresca constitutive model both options for incorporating partial material factors in numerical analysis (i.e. strength-reduction approaches SR1 and SR2) result in the same failure loads for the same partial factor. Additional analyses, not presented here, also indicate that the results are not dependent on the value of K_0, as would be expected.

Analysis results with MCC model

Two sets of analyses have been performed with this model: one adopting $K_0 = 1$ throughout and the other adopting the Jaky (1948) expression for $K_0 = 1 - \sin\phi'$. The set of analyses that adopts the K_0 value of 1 is described first, with other model parameters as given in Table 2 and assuming normally consolidated conditions in the soil (i.e. OCR = 1). As before, the solid line in Fig. 3 shows the load–settlement behaviour of the footing when the characteristic strength $\phi'_{ch} = 30°$ is adopted at the beginning of the analysis. It results in the ultimate footing load of 32·7 kN.

The second analysis also starts with $\phi'_{ch} = 30°$, and the footing is loaded initially to a working load of 22·1 kN (i.e. $L_f = 1{\cdot}5$). This load is then maintained while the soil strength is gradually reduced according to the SR1 approach, resulting in further footing settlement. The corresponding load–displacement curve is a solid line with symbols, and the resulting partial material factor is $\gamma_m = 1{\cdot}6$.

The third analysis then adopts the factored strength from the beginning of the analysis (strength reduction SR2 and γ_m obtained in the previous analysis), which gives $\phi'_d = 19{\cdot}8°$ (= arctan(tan30°/1·6)). The dashed line in Fig. 3 shows this load–displacement curve, which indicates the same failure load as the previous analysis, for the same partial material factor of 1·6.

Consequently, as with the Tresca model, the analyses using the MCC model and adopting $K_0 = 1$ predict the same failure load with both the SR1 and SR2 strength-reduction approaches.

The second set of analyses adopts the same model parameters, characteristic strength and normally consolidated soil conditions, but K_0 is now calculated from $1 - \sin\phi'$, and therefore depends on the magnitude of the angle of shearing resistance.

As before, the first analysis adopts $\phi'_{ch} = 30°$, which results in $K_0 = 0{\cdot}5$ and the load–displacement curve in Fig. 4 shown by the solid line, indicating the maximum footing load of 29 kN.

In the second analysis $\phi'_{ch} = 30°$ and $K_0 = 0{\cdot}5$ are adopted at the beginning of the analysis, and the footing is loaded to a working load of 14·5 kN (i.e. $L_f = 2$). The load is then maintained at this level, and the soil strength is reduced until failure of the footing (SR1 approach), leading to further footing settlement. The resulting partial material factor is 2·25.

The third analysis now starts with a reduced (i.e. design) strength $\phi'_d = 14{\cdot}4°$ (= arctan(tan30°/2·25)), but there is a dilemma as to the choice of the value of K_0. If $K_0 = 0{\cdot}751$ is adopted, which is consistent with the modified value of ϕ' (i.e. $= 1 - \sin 14{\cdot}4°$), then the dashed line in Fig. 4 is obtained for the resulting load–displacement curve, indicating the ultimate footing load of 17·1 kN. This is different from 14·5 kN in the above SR1 approach. If this analysis is then repeated with the same reduced strength of $\phi'_d = 14{\cdot}4°$, but adopting the original $K_0 = 0{\cdot}5$ value in the initial stresses, then the dot-dashed line in Fig. 4 is obtained for the load–settlement curve, and the maximum footing load is 27·6 kN. This result is also different from 14·5 kN. In addition, this load–settlement curve initially develops a slight negative reaction.

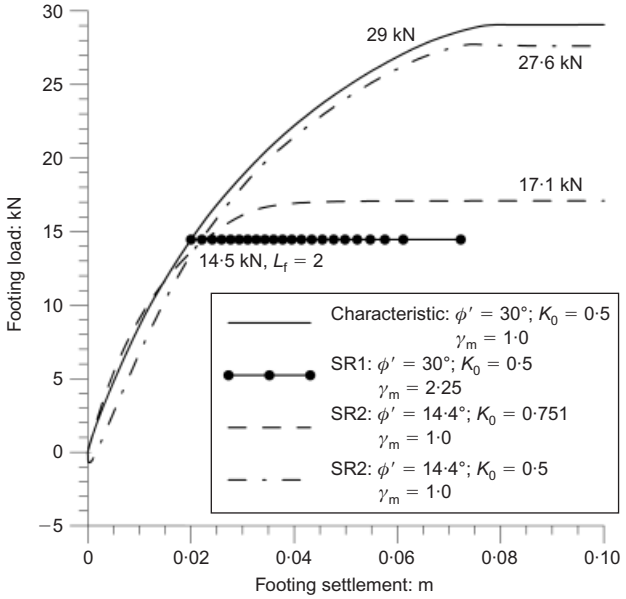

Fig. 4. Load–settlement curves for undrained footing capacity using MCC model and $K_0 \neq 1$

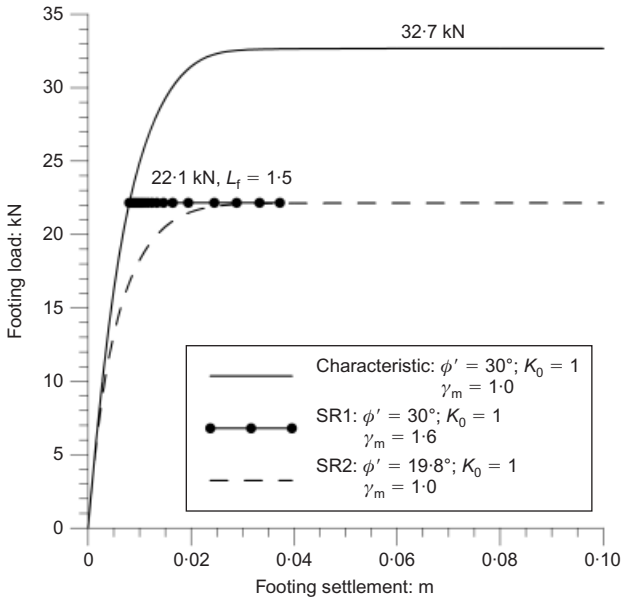

Fig. 3. Load–settlement curves for undrained footing capacity using MCC model and $K_0 = 1$

Discussion of the MCC results

First, it is evident from the above that the MCC model does not always produce the same result for the same γ_m with the two strength-reduction approaches, and that this appears to depend on the value of K_0.

$K_0 = 1$ is a special case in which the initial state of stresses in the ground is isotropic. This implies that, as OCR = 1, the initial hardening parameter p'_0 in equation (35) (see Appendix) at any depth is dependent only on the isotropic stress p', and not on the shape of the yield surface, and hence on $g(\theta)$ and ϕ'. This results in the specific volume at any particular depth being the same in both strength-reduction calculations, and hence results in the same failure conditions for a given problem, independent of how the partial material factor is applied.

However, when K_0 is not 1, it is observed that the two analyses (with the same factored strength ϕ'_d, but different K_0 values) performed with the SR2 strength-reduction approach result in different ultimate loads, and that these are also different from the ultimate conditions obtained with the SR1 strength-reduction approach. The former observation can be explained by scrutinising the expression for the undrained strength that can be derived for this model from

its input parameters and initial stresses (see Potts & Zdravkovic, 1999, for details of this derivation)

$$S_u = \sigma'_{vi} \cdot g(\theta) \cdot \cos\theta \cdot \frac{1+2K_0}{3} \cdot \left(\frac{1+B^2}{2}\right)^{1-\kappa/\lambda} \quad (28)$$

where

$$B = \frac{\sqrt{3}(1-K_0)}{g(-30°)(1+2K_0)}$$

and

$$g(\theta) = \frac{\sin\phi'}{\cos\theta + \frac{\sin\theta\sin\phi'}{\sqrt{3}}}$$

where σ'_{vi} is the initial vertical effective stress (i.e. at the beginning of the analysis); $g(\theta)$ is the inclination of the critical-state line; and all other parameters are as introduced before.

It is clear from equation (28) that the magnitude of K_0 influences the magnitude of S_u, and Fig. 5 shows the undrained strength profiles for these two analyses, which are in agreement with the magnitudes of the ultimate footing loads shown in Fig. 4 (i.e. the higher undrained strength of the SR2 approach with $K_0 = 0{\cdot}5$ results in a higher ultimate load).

The latter observation is explained by recognising that these three undrained analyses are also performed at different initially established specific volumes. This arises, in contrast to the $K_0 = 1$ case, because these analyses have an anisotropic initial stress state in the ground (i.e. initial deviatoric stress $J_{in} \neq 0$). Consequently, when calculating the initial hardening parameter p'_0, again with OCR = 1, the initial stress state (J_{in}, p'_{in}) and the shape of the yield surface, which depends on $g(\theta)$ and ϕ', affect its magnitude. The undrained strength mobilised at failure in the analysis with the SR1 approach is the smallest (Fig. 5), and therefore results in the smallest ultimate load for the same partial material factor (Fig. 4). Also shown in these two figures are the undrained strength profile for the analysis with the characteristic (unfactored) strength and the resulting ultimate load respectively.

Second, the initial negative reaction on the footing in the MCC analysis with $\phi'_d = 14{\cdot}4°$ and $K_0 = 0{\cdot}5$ results from the initial conditions in the soil being on the dry side of the critical state for this combination of parameters. In this respect, Fig. 6 shows the initial profiles of the mean effective stress p' and the deviatoric stress J, which are of constant gradients and give a constant stress ratio J/p' at the beginning of this analysis of 0·433. This is a higher gradient than the inclination of the critical-state line $g(\theta)$, which for the factored strength $\phi'_d = 14{\cdot}4°$ and the initial $\theta = -30°$ equals 0·313. Consequently, as sketched in Fig. 6 for the example stress state at 10 m depth (point A), the initial stresses in the ground are on the dry side of the critical state. Therefore, on initial application of footing load, there is some undrained softening in the load–displacement curve. Although this is consistent with the assumed OCR and the initial stress conditions, it is not particularly realistic.

In the analysis with $\phi'_d = 14{\cdot}4°$ and $K_0 = 0{\cdot}751$, the initial stress ratio $J/p' = 0{\cdot}172$, which is a lower gradient than that of the critical-state line (= 0·313). Consequently, the initial state for this analysis is on the wet side of the critical state, and is therefore in agreement with the assumption of normal consolidation.

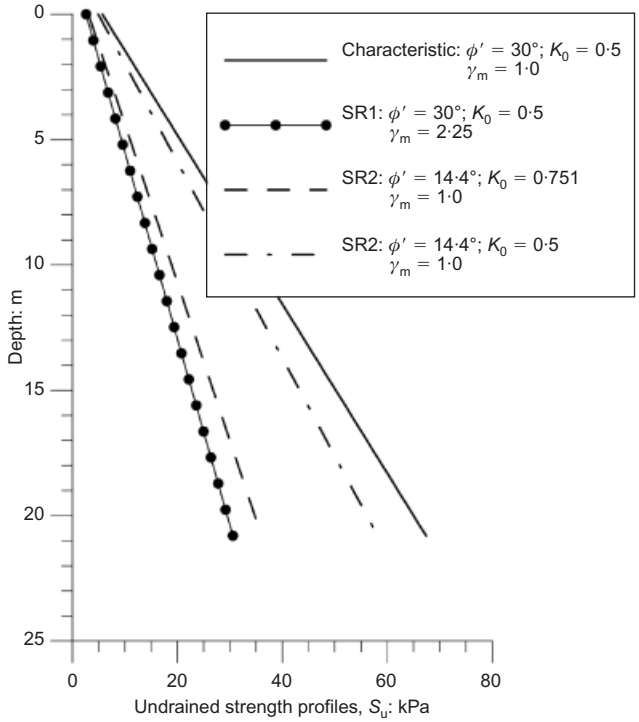

Fig. 5. Undrained strength profiles for MCC bearing capacity analyses with $K_0 \neq 1$

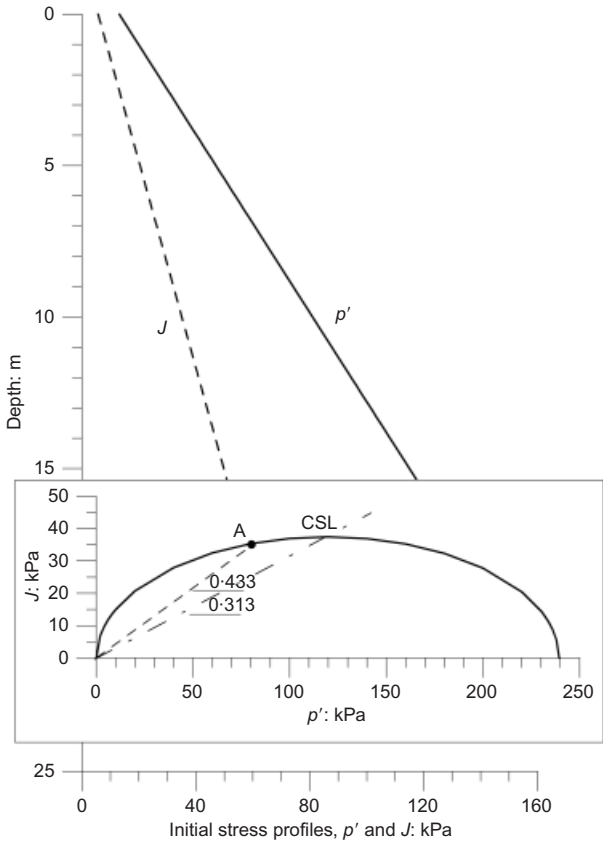

Fig. 6. Initial stresses in the ground in MCC analysis with $\phi'_d = 14{\cdot}4°$ and $K_0 = 0{\cdot}5$

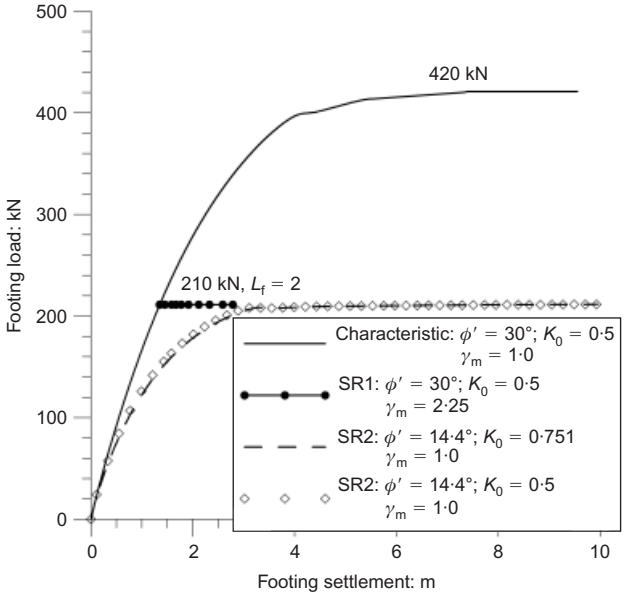

Fig. 7. Load–settlement curves for drained footing capacity using MCC model

DRAINED BEARING CAPACITY

The drained bearing capacity of the strip footing in Fig. 1 has been analysed with the MCC and Lade's single-hardening constitutive models.

Analyses with MCC model

The set of analyses performed here adopts the same ground conditions as the previous undrained bearing capacity analyses, $\phi'_{ch} = 30°$ and Jaky's expression for K_0 in the ground. Therefore, in the first analysis $\phi'_{ch} = 30°$ and $K_0 = 0·5$, resulting in the load–displacement curve in Fig. 7 shown as a solid line and the maximum footing load of 420 kN.

In the second analysis the same initial conditions are adopted, of $\phi'_{ch} = 30°$ and $K_0 = 0·5$, and the footing is loaded initially to 210 kN (i.e. load factor $L_f = 2$). A gradual increase of the partial material factor at the constant load of 210 kN reduces ϕ'_{ch} gradually according to the SR1 strength-reduction procedure, until footing failure occurs at $\gamma_m = 1·3$.

The third analysis starts with the factored strength (strength reduction SR2), such that $\phi'_d = \arctan(\tan 30°/1·3) = 24°$ and the corresponding $K_0 = 1 - \sin 24° = 0·594$. The dashed line in Fig. 7 shows the load–displacement curve from this analysis, which reaches the ultimate load of 210 kN for $\gamma_m = 1·3$. This load is the same as in the SR1 approach above.

For completeness, a fourth analysis is performed that also starts with the factored strength $\phi'_d = 24°$, but adopts $K_0 = 0·5$, which corresponds to the unfactored soil strength. The resulting load–settlement curve plots very close to that from the third analysis, and is therefore shown with open symbols in Fig. 7.

Contrary to the undrained bearing capacity results with the MCC model, the drained analyses have demonstrated that both strength-reduction approaches with this model result in the same bearing capacity of the footing for the same partial material factor. This is not surprising, as MCC is characterised by the drained soil's strength in terms of the angle of shearing resistance, which has a constant value in the model. Although not shown here, a similar result is obtained if a simple Mohr–Coulomb model is used to simulate the soil. Again the results are independent of K_0, as would be expected.

Analyses with Lade's single-hardening model

As explained in the Appendix, Lade's model is formulated in terms of effective stress, but does not include the angle of shearing resistance ϕ' as an input parameter. Instead, the peak strength is controlled by several of the input parameters. As a result, ϕ' varies with stress level. In the original formulation of the model (Kim & Lade, 1988), once the peak strength is reached, strain-softening behaviour occurs, and the strength reduces to zero at very large strains. To overcome this unrealistic reduction in strength, the version of the model implemented in ICFEP allows the strength to reduce from peak to an ultimate value. However, in the analyses presented in this paper the peak and ultimate strengths were set equal so that no strain-softening occurs. This avoids any problems with mesh dependence (i.e. objectivity), and results in the load–displacement curves for the footing reaching a well-defined plateau.

The implication of the above is that in the footing analyses the angle of shearing resistance is dependent on stress level, varying with both mean effective stress and Lode angle. Consequently, when applying the SR1 strength-reduction approach, it is necessary to account for this variation and adopt a particular Lode angle at which the partial factor is to be applied. Here it has been assumed that it is the angle of shearing resistance in triaxial compression that is factored. For further details see the Appendix.

Following the same methodology as described so far, the first analysis of the bearing capacity problem with Lade's model adopts the characteristic (unfactored) soil strength, which is represented with a strength input parameter $\eta_{1,ch} = 24·7$ (see Table 3), and the footing is loaded to failure. The resulting initial variation with depth of the angle of shearing resistance, which is available in the ground before application of the footing loading, is shown in Fig. 8. The relationship is highly non-linear, with ϕ' varying from about 38° at the ground surface (i.e. lower stress levels) to about 33·5° at 20 m depth (i.e. higher stress levels). Because

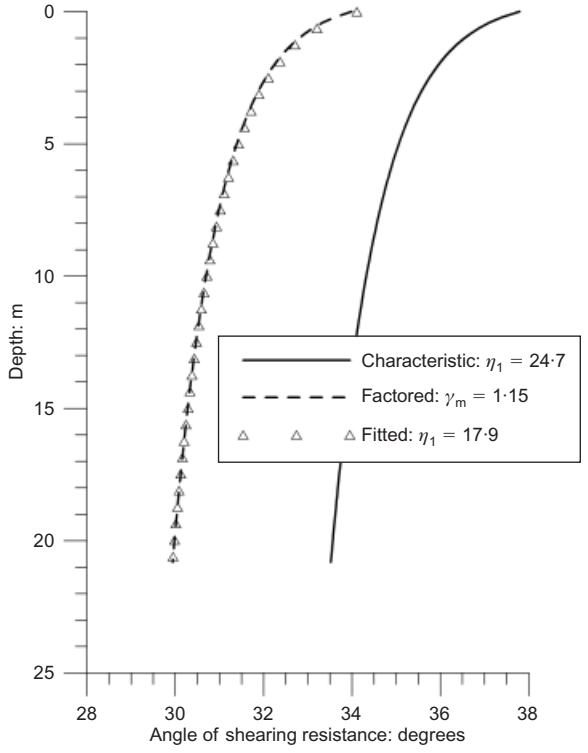

Fig. 8. Distributions of angle of shearing resistance in soil for analyses with Lade's single-hardening model

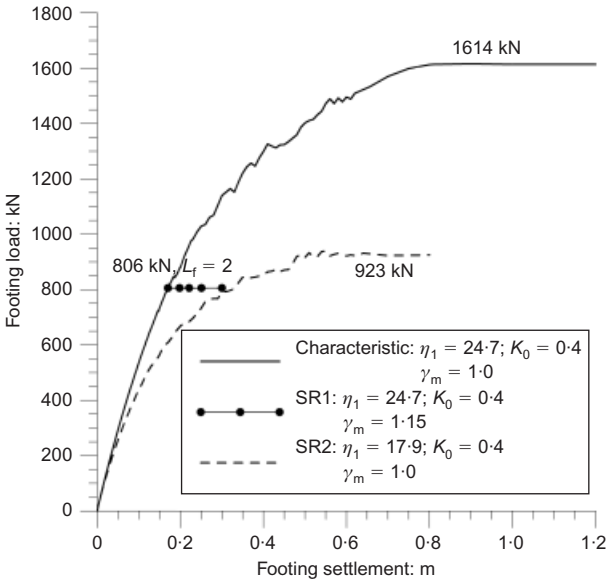

Fig. 9. Load–settlement curves for drained bearing capacity using Lade's single-hardening model

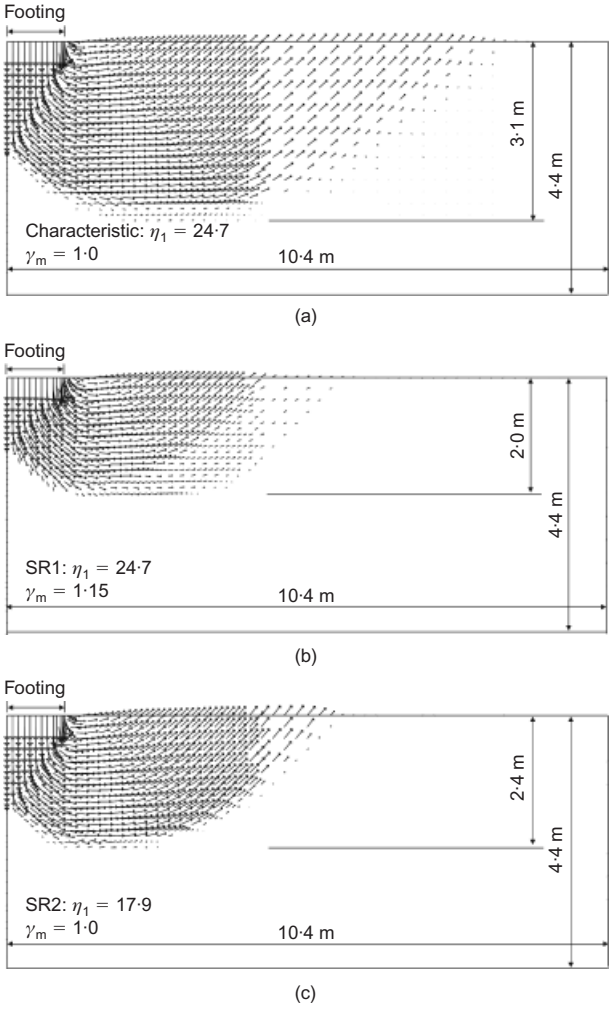

Fig. 10. Mechanisms of ground failure under footing for (a) characteristic strength, (b) strength reduction SR1 and (c) strength reduction SR2, using Lade's single-hardening model

of this variation, Jaky's formula is not applied for calculating K_0; instead a constant value of $K_0 = 0{\cdot}4$ is adopted in all analyses. The resulting load–displacement curve from this first analysis is shown as the solid line in Fig. 9, which indicates the maximum footing load at failure of 1614 kN.

The second analysis starts with the same characteristic strength and other ground conditions, and the footing is loaded to 806 kPa (load factor $L_f = 2$). This load is then maintained while the soil's strength is reduced (strength reduction SR1), resulting in a failure of the footing when $\gamma_m = 1{\cdot}15$ is achieved.

In the third analysis it is now not possible to factor a single value of ϕ' (strength reduction SR2), as in the drained MCC analysis, as ϕ' varies with depth. Therefore $\gamma_m = 1{\cdot}15$ from the second analysis is applied on the whole distribution of the characteristic angle of shearing resistance in Fig. 8, which results in the factored initial strength of the soil, at the beginning of the third analysis, as shown by the dashed line in Fig. 8. Since ϕ' is not an input parameter to the model, the strength parameter η_1 is reduced iteratively until the same distribution of ϕ' is obtained. This distribution is shown by symbols in Fig. 8 (which plot on top of the dashed line), and the resulting $\eta_{1,d} = 17{\cdot}9$. The ultimate load on the footing from this analysis (load–displacement curve shown as a dashed line in Fig. 9) is 923 kN, which is different from 806 kN in the SR1 strength-reduction approach.

Contrary to the drained bearing capacity results with the MCC model, the two strength-reduction approaches applied in the drained bearing capacity calculations with Lade's model do not result in the same footing capacity for the same partial material factor. The reason for this is the non-linear variation of the angle of shearing resistance with stress level in the formulation of this model, which has resulted in different failure mechanisms mobilised in the soil for the two approaches. Fig. 10 shows vectors of ground movement at failure for all three analyses performed with Lade's model. The relative magnitudes and directions of the vectors indicate the extent of the mobilised volume of soil. The mechanism in Fig. 10(a) is for the analysis with the characteristic soil strength, which resulted in the largest load on the footing (1614 kN). Therefore this is the deepest mechanism (3·1 m) and has the largest lateral extent, with the maximum mobilised ϕ' within this volume of soil of 40°. Strength-reduction approach SR1 results in the failure mechanism shown in Fig. 10(b), which has the smallest volume (maximum depth of 2·0 m) and the maximum mobilised ϕ' of 33·4°. Finally, strength-reduction approach SR2 results in the failure mechanism shown in Fig. 10(c), which is of larger extent than the SR1 mechanism (maximum depth of 2·4 m), and mobilises a maximum ϕ' of 36·3° and hence a larger footing capacity.

CONCLUSIONS

The combination of design codes such as EC7, which require, among other design changes, the application of partial factors on soil strength, with an increased use of advanced numerical methods in geotechnical design, has made it necessary for the numerical analysis to be able to account for these partial factors. The soil strength can be reduced by the partial factor in two ways, either at the beginning of the analysis (SR2) or at some stage during the analysis (SR1), the latter approach being more difficult, as it requires changes in the numerical software.

There is currently no guidance as to which of the two approaches is more appropriate to apply, nor on how the SR1 approach should be implemented in the numerical procedure. With respect to the latter, this paper presents a consistent numerical procedure that can be applied in any numerical software and with any constitutive model. The

former issue is then investigated on the example of the bearing capacity of a footing, by applying both strength-reduction approaches with a selection of constitutive models.

In the proposed procedure, strength-reduction approach SR1 involves the introduction of a partial material factor as an additional state parameter in the yield function of the constitutive model. The paper shows that the necessary modifications to the finite-element formulation, in terms of the governing equations and the relationship between the changes in stresses and strains, are relatively straightforward. In addition to the usual derivatives of the yield and plastic potential functions in terms of stresses and state parameters, these modifications require a derivative of the yield function with respect to the partial material factor. The paper shows how the latter can be derived on examples of constitutive models that involve both a constant strength, which is the model input parameter (S_u or ϕ'), and a strength that varies in a non-linear manner (e.g. with stress level) and is not the model input parameter.

Finally, by utilising both the SR1 and SR2 strength-reduction procedures on the bearing capacity problem of a surface footing, the paper investigates their applicability in predicting the ultimate limit states for a given partial material factor. In this respect it is shown that, for a simple constitutive model such as Tresca, the two approaches predict the same ultimate states for the same partial material factor. However, with more advanced models this is not necessarily the case, as shown with the undrained bearing capacity calculations using the MCC model and drained bearing capacity using Lade's model. In some situations, as in the undrained bearing capacity analyses with the MCC model, the use of strength reduction at the beginning of the analysis (SR2) may lead to unrealistic predictions. In addition, this approach may be difficult to apply with constitutive models that have strength dependent on stress and/or strain level. It would appear that only strength reduction SR1 (at some stage in the analysis) can be applied consistently with any constitutive model for determination of the partial factor for a given problem.

Only results for the bearing capacity problem have been presented in this paper. Although this may be considered a simple boundary value problem, it demonstrates the complexities and difficulties that can be encountered when combining partial factors with numerical analysis. Further research is required to investigate the use of partial factors in other boundary value problems analysed using numerical methods.

APPENDIX

For applications presented in this paper, the Tresca and MCC constitutive models are formulated in the general stress space in terms of stress invariants p (the mean stress), J (the deviatoric stress) and θ (Lode angle), whereas Lade's single-hardening model is generalised in terms of stress invariants I_1, I_2 and I_3. Details of all the models can be found in Potts & Zdravkovic (1999). Here, apart from the basic equations of the three yield functions, only the derivatives of the yield function with respect to the partial material factor for each model are presented, which are necessary for the implementation of strength-reduction approach SR1 in finite-element software.

Stress invariants

$$\begin{aligned} I_1 &= \sigma_1 + \sigma_2 + \sigma_3 \\ I_2 &= \sigma_1\sigma_2 + \sigma_2\sigma_3 + \sigma_3\sigma_1 \\ I_3 &= \sigma_1\sigma_2\sigma_3 \end{aligned} \tag{29}$$

$$\begin{aligned} p &= \tfrac{1}{3}(\sigma_1 + \sigma_2 + \sigma_3) \\ J &= \frac{1}{\sqrt{6}}\sqrt{(\sigma_1-\sigma_2)^2 + (\sigma_2-\sigma_3)^2 + (\sigma_3-\sigma_1)^2} \\ \theta &= \arctan\left\{\frac{1}{\sqrt{3}}\left[2\left(\frac{\sigma_2-\sigma_3}{\sigma_1-\sigma_3}\right) - 1\right]\right\} \end{aligned} \tag{30}$$

Tresca model

Tresca yield function:

$$F = J\cos\theta - S_{u,d} = 0 \tag{31}$$

where J and θ represent the current stress state. The strength parameter in the Tresca model is the undrained strength S_u, and this is the quantity that is modified by the partial factor: that is

$$S_{u,d} = \frac{S_{u,ch}}{\gamma_m} \tag{32}$$

Therefore, after combining equation (31) and equation (32)

$$F = \frac{J\cos\theta \cdot \gamma_m}{S_{u,ch}} - 1 = 0 \tag{33}$$

$$\frac{\partial F}{\partial \gamma_m} = \frac{J\cos\theta}{S_{u,ch}} = \frac{1}{\gamma_m} \tag{34}$$

Modified Cam Clay (MCC) model

MCC yield function:

$$F = \left[\frac{J}{p'g(\theta)}\right]^2 - \left(\frac{p'_0}{p'} - 1\right) = 0 \tag{35}$$

where p'_0 is the hardening parameter representing the size of the yield surface; p' and J represent the current stress state; and $g(\theta)$ is the gradient of the critical-state line, which, for the adopted Mohr–Coulomb hexagon shape of the yield surface in the deviatoric plane in this study, is

$$g(\theta) = \frac{\sin\phi'_d}{\cos\theta + (\sin\theta\sin\phi'_d/\sqrt{3})} \tag{36}$$

The strength parameter in the MCC model is the angle of shearing resistance ϕ', and therefore this is the parameter that is modified by the partial factor

$$\tan\phi'_d = \frac{\tan\phi'_{ch}}{\gamma_m} \tag{37}$$

The derivative of the yield function with respect to γ_m is calculated as

$$\frac{\partial F}{\partial \gamma_m} = \frac{\partial F}{\partial g(\theta)}\frac{\partial g(\theta)}{\partial \phi'_d}\frac{\partial \phi'_d}{\partial \gamma_m} \tag{38}$$

From the above equations

$$\frac{\partial F}{\partial g(\theta)} = -\frac{2}{g(\theta)}\left[\frac{J}{p'g(\theta)}\right]^2 \tag{39}$$

$$\frac{\partial g(\theta)}{\partial \phi'_d} = \frac{[g(\theta)]^2}{\tan\phi'_d}\frac{\cos\theta}{\sin\phi'_d} \tag{40}$$

$$\frac{\partial \phi'_d}{\partial \gamma_m} = -\frac{\sin\phi'_d\cos\phi'_d}{\gamma_m} \tag{41}$$

Substituting equations (39)–(41) into equation (38) gives

$$\frac{\partial F}{\partial \gamma_m} = \frac{2g(\theta)}{\gamma_m}\left[\frac{J}{p'g(\theta)}\right]^2\frac{\cos\theta\cos\phi'_d}{\tan\phi'_d} \tag{42}$$

Lade's single-hardening model

Lade's yield function:

$$F = \left(\psi_1\frac{I_1^3}{I_3} - \frac{I_1^2}{I_2}\right)\left(\frac{I_1}{p_a}\right)^h \exp(q) - F''(W_p) = 0 \tag{43}$$

where

$$\psi_1 = 0{\cdot}00155\,m^{-1{\cdot}57}$$

$$q = \frac{\alpha S}{1-(1-\alpha)S}$$

$$S = \frac{\eta}{\eta_1} = \frac{1}{\eta_1}\left(\frac{I_1^3}{I_3} - 27\right)\left(\frac{I_1}{p_a}\right)^m$$

and W_p is the plastic work, with the $F''(W_p)$ expression depending on whether the material is hardening or softening.

This yield surface is curved in any plane containing the hydrostatic axis, and its shape in the deviatoric plane is a smoothly rounded triangle. Parameters m and ψ_1 control the roundness of the surface, whereas its curvature is defined by parameters h and q. The parameter q varies with stress level S from zero at the hydrostatic axis to unity at the failure surface, and η_1 is the strength parameter.

In this model the angle of shearing resistance ϕ' is no longer constant but depends on the stress ratio at failure, $(J/p')^f = g(\theta) = \sqrt{J_{2\eta}^f}$, which is obtained as a solution of the following cubic equation for the Lade's surface in the deviatoric plane

$$\frac{2}{\sqrt{27}}\sin(3\theta)\left(\sqrt{J_{2\eta}^f}\right)^3 + \left(\sqrt{J_{2\eta}^f}\right)^2 - \frac{(\eta_1/27)(p_a/I_1)^m}{1+(\eta_1/27)(p_a/I_1)^m} = 0 \tag{44}$$

Consequently, $\partial F/\partial\gamma_m$ for this model can be calculated as

$$\frac{\partial F}{\partial \gamma_m} = \frac{\partial F}{\partial \phi_d'}\frac{\partial \phi_d'}{\partial \gamma_m} = \frac{\partial F}{\partial q}\frac{\partial q}{\partial S}\frac{\partial S}{\partial \eta_1}\frac{\partial \eta_1}{\partial\left(\sqrt{J_{2\eta}^f}\right)}\frac{\partial\left(\sqrt{J_{2\eta}^f}\right)}{\partial\left[g(\theta)\right]}\frac{\partial\left[g(\theta)\right]}{\partial \phi_d'}\frac{\partial \phi_d'}{\partial \gamma_m} \tag{45}$$

In the above derivations the assumption is that the partial factor is applied to ϕ' in triaxial compression, and therefore $\theta = -30°$ is used in equation (45).

From equation (43)

$$\frac{\partial F}{\partial q} = \left(\psi_1\frac{I_1^3}{I_3} - \frac{I_1^2}{I_2}\right)\left(\frac{I_1}{p_a}\right)^h \exp(q) \tag{46}$$

$$\frac{\partial q}{\partial S} = \frac{q^2}{\alpha S^2} \tag{47}$$

$$\frac{\partial S}{\partial \eta_1} = -\frac{S}{\eta_1} \tag{48}$$

From equation (44)

$$\frac{\partial \eta_1}{\partial\left(\sqrt{J_{2\eta}^f}\right)} = \left[\frac{6}{\sqrt{27}}\sin 3\theta\left(\sqrt{J_{2\eta}^f}\right)^2 + 2\sqrt{J_{2\eta}^f}\right]\frac{\left[1+\frac{\eta_1}{27}\left(\frac{p_a}{I_1}\right)^m\right]^2}{\frac{1}{27}\left(\frac{p_a}{I_1}\right)^m} \tag{49}$$

$$\frac{\partial\left(\sqrt{J_{2\eta}^f}\right)}{\partial\left[g(\theta)\right]} = 1 \tag{50}$$

and the last two derivatives in equation (45) are the same as already given for the MCC model in equations (40) and (41). Substituting equations (40), (41) and (46)–(50) into equation (45), the derivative of Lade's yield function with respect to the partial factor is obtained.

This model can also account for an attraction and therefore implicitly for a cohesion in the soil. In such a situation further differentiations are necessary (i.e. $(\partial F/\partial c')(\partial c'/\partial\gamma_m)$), but as no attraction has been adopted in the model parameters for the footing analyses, these differentiations are not presented here.

Furthermore, the model can be extended to account for a post-peak softening by adopting an additional strength parameter, η_{cs}, in the model formulation and setting it to be greater than zero and smaller than η_1. This again requires additional differentiations with respect to the partial material factor, but as the footing study considers only a pre-peak behaviour of the sand (i.e. $\eta_{cs} = \eta_1$), they are not presented here.

NOTATION

A	base area of footing
$[B]$	matrix of derivatives of shape functions
C	work-hardening parameter in Lade's model
c'	cohesion
c'_{ch}	characteristic cohesion
c'_d	design cohesion
$[D]$	elastic matrix
$[D]^{ep}$	elasto-plastic constitutive matrix
$\{\Delta d\}$	vector of displacements
$\{\Delta d\}_n$	vector of nodal displacements
E	total potential energy
F	yield function
$\{\Delta F\}$	vector of body forces
g	plastic potential exponent in Lade's model
$g(\theta)$	inclination of critical-state line
h	yield exponent in Lade's model
I_1, I_2, I_3	stress invariants
J	deviatoric stress
J_{in}	initial deviatoric stress
$J_{2\eta}^f$	square of stress ratio at failure in Lade's model
K_0	coefficient of earth pressure at rest
$[K_E]$	element stiffness matrix
$\{k\}$	vector of state parameters in yield function
L	work done by applied loads
L_f	load factor
M	Young's modulus coefficient in Lade's model
m	failure exponent in Lade's model
$\{m\}$	vector of state parameters in plastic potential function
N	number of elements
$[N]$	matrix of shape functions
N_c	bearing capacity factor
OCR	overconsolidation ratio
P	plastic potential function
p	mean stress
p	work-hardening exponent in Lade's model
p'	mean effective stress
p_a	atmospheric pressure
p'_{in}	initial mean effective stress
p'_0	initial hardening parameter in MCC model
Q_f	ultimate load on footing
q	parameter in Lade's model
$\{\Delta R_E\}$	right-hand-side load vector
S	stress level
S_u	undrained strength
$S_{u,ch}$	characteristic undrained strength
$S_{u,d}$	design undrained strength
Srf	part of boundary of domain over which surface tractions are applied
$\{\Delta T\}$	vector of surface tractions
v_1	specific volume at unit mean effective stress
Vol	volume of domain
W	strain energy
W_p	plastic work in Lade's model
α	yield parameter in Lade's model
γ	bulk unit weight
γ_m	partial material factor
$\{\Delta\varepsilon\}$	vector of total strains
$\{\Delta\varepsilon^e\}$, $\{\Delta\varepsilon^p\}$	elastic and plastic components strains
η	mobilised strength in Lade's model
η_{cs}	critical state strength parameter in Lade's model
η_1	peak strength parameter in Lade's model
$\eta_{1,ch}$	characteristic strength parameter in Lade's model
$\eta_{1,d}$	design strength parameter in Lade's model
θ	Lode angle
κ	inclination of swelling lines in v–$\ln p'$ space in MCC model
Λ	scalar multiplier

λ inclination of virgin compression line in $v-\ln p'$ space in MCC model
λ Young's modulus exponent in Lade's model
μ Poisson's ratio
$\{\sigma\}$ stress vector
$\{\sigma_c\}$ correction vector
σ'_{vi} initial vertical effective stress
ψ_1 parameter in Lade's model
ψ_2 plastic potential coefficient in Lade's model
ϕ' angle of shearing resistance
ϕ'_{ch} characteristic angle of shearing resistance
ϕ'_d design angle of shearing resistance

REFERENCES

Bauduin, C., De Vos, M. & Simpson, B. (2000). Some considerations on the use of finite element methods in ultimate limit state design. *Proc. Int. Workshop on Limit State Design in Geotech. Engng, Melbourne, Australia*, 31–46 (CD-ROM).

Bauduin, C., De Vos, M. & Frank, R. (2003). ULS and SLS design of embedded walls according to Eurocode 7. *Proc. 13th Eur. Conf. Soil Mech. Geotech. Engng, Prague* **2**, 41–46.

Brinkgreve, R. B. J. & Bakker, H. L. (1991). Non-linear finite element analysis of safety factors. *Proc. 7th IACMAG Conf., Cairns*, 1117–1122.

Cheung, K., West, K., Yeow, H. & Simpson, B. (2010). Do Eurocodes make a difference? *Geomech. Tunnelling* **3**, No. 1, 35–47.

Jaky, J. (1948). Pressure in soils. *Proc. 2nd Int. Conf. Soil Mech. Found. Engng, London* **1**, 103–107.

Kim, M. K. & Lade, P. V. (1988). Single hardening constitutive model for frictional materials: I. Plastic potential function. *Comput. Geotech.* **5**, No. 4, 307–324.

Kovacevic, N. (1994). *Numerical analysis of rockfill dams, cut slopes and road embankments*. PhD thesis, Imperial College, University of London, UK.

Lade, P. V. & Kim, M. K. (1988). Single hardening constitutive model for frictional materials: II. Yield criterion and plastic work contours. *Comput. Geotech.* **6**, No. 1, 13–29.

Potts, D. M. & Zdravkovic, L. (1999). *Finite element analysis in geotechnical engineering: theory*. London, UK: Thomas Telford.

Potts, D. M. & Zdravkovic, L. (2011). Application of partial factors of safety in numerical analysis of bearing capacity. *Proc. 2nd Int. Symp. on Computational Geomech. (ComGeo II), Dubrovnik* (CD-ROM).

Roscoe, K. H. & Burland, J. B. (1968). On the generalised stress–strain behaviour of wet clay. In *Engineering plasticity* (eds J. Heyman and F. A. Leckie), pp. 535–609. Cambridge, UK: Cambridge University Press.

Schweiger, H. (2005). Application of FEM to ULS design (Eurocodes) in surface and near surface geotechnical structures. *Proc. 11th Int. Conf. of IACMAG, Turin*, 419–430.

Schweiger, H., Marcher, T. & Nasekhian, A. (2010). Nonlinear FE analysis of tunnel excavation: comparison of EC7 design approaches. *Geomech. Tunnelling* **3**, No. 1, 61–67.

Simpson, B. (2000). Partial factors: where to apply them? *Proc. Int. Workshop on Limit State Design in Geotech. Engng, Melbourne, Australia* (CD-ROM).

Simpson, B. (2007). Approaches to ULS design: the merits of Design Approach 1 in Eurocode 7. *Proc. 1st Int. Symp. on Geotech. Safety and Risk, Shanghai*, 527–538.

Zdravkovic, L. Potts, D. M. & Jackson, C. (2003). Numerical study of the effect of pre-loading on undrained bearing capacity. *ASCE Int. J. Geomech.* **3**, No, 1–2, 1–10.